SCIENCE CHINA
Information Sciences

• RESEARCH PAPER •

April 2026, Vol. 69, Iss. 4, 142205:1–142205:16
https://doi.org/10.1007/s11432-024-4807-5

Robust model predictive control for perturbed nonlinear multi-agent systems via dynamic event-triggered scheme

Rui GUO[1,2], Jianwen FENG[3*], Yi ZHAO[3], Tingwen HUANG[4], Xinzhi LIU[5] & Jingyi WANG[3*]

[1]*College of Computer Science and Software Engineering, Shenzhen University, Shenzhen 518060, China*
[2]*College of Mechatronics and Control Engineering, Shenzhen University, Shenzhen 518060, China*
[3]*School of Mathematical Sciences, Shenzhen University, Shenzhen 518060, China*
[4]*Faculty of Computer Science and Control Engineering, Shenzhen University of Advanced Technology, Shenzhen 518055, China*
[5]*Department of Applied Mathematics, University of Waterloo, Waterloo N2L 3G1, Canada*

Received 2 August 2024/Revised 5 March 2025/Accepted 9 October 2025/Published online 10 March 2026

Abstract A model predictive control approach integrated with a dynamic event-triggered strategy is investigated to address the formation stabilization problem of nonlinear multi-agent systems subject to input constraints and additive disturbances. Specifically, a dynamic-type event-triggered mechanism is proposed, in which the triggering threshold is dynamically adjusted within a predefined interval by a dynamic variable. Under this mechanism, the optimization problem is solved only at triggering instants, significantly reducing computational resources while ensuring satisfactory system performance. In addition, a prediction horizon shrinkage strategy is introduced within the model predictive control framework, along with the formulation of a robustness constraint. Consequently, the designed optimization problem achieves reduced computational complexity while effectively handling external disturbances. Through rigorous analysis, theoretical results are established to ensure the recursive feasibility of the overall algorithm and the stability of the resulting closed-loop system. Finally, a numerical example and comparative studies with existing approaches are presented to demonstrate the effectiveness and superiority of the proposed method.

Keywords nonlinear multi-agent systems, dynamic event-triggered mechanism, model predictive control, robust control

Citation Guo R, Feng J W, Zhao Y, et al. Robust model predictive control for perturbed nonlinear multi-agent systems via dynamic event-triggered scheme. Sci China Inf Sci, 2026, 69(4): 142205, https://doi.org/10.1007/s11432-024-4807-5

1 Introduction

Over the past few decades, multi-agent systems (MASs) have attracted extensive attention from both academia and industry due to their superior scalability, reliability, and efficiency in contrast to a single-agent system [1, 2]. Such systems can model a wide range of real-world networks, e.g., satellite fleets [3, 4], social networks [5, 6], intelligent traffic systems [7, 8], and power systems [9, 10]. Consequently, the research on the coordinated control of MASs is of theoretical and extensive significance.

Among the noteworthy investigations for MASs, model predictive control (MPC) has emerged as an appealing control method due to its effectiveness in dealing with multivariable and complex constraints [11, 12]. Considering that MPC is an optimization-based approach, a crucial challenge is how to implement MPC in resource-limited scenarios. Related to this, the event-triggered mechanism, being a resource-saving and extensible strategy, presents a promising solution to decrease resource consumption without compromising system performance [13–15]. Under the traditional framework of event-triggered model predictive control (ETMPC), optimization problems are solved only when a well-defined deviation exceeds a prescribed threshold [16]. Therefore, unnecessary computation loads are efficiently avoided and resource consumption is remarkably lessened. To date, several notable event-triggered strategies for MPC have been investigated in the literature, such as static ETMPC [16–18], dynamic ETMPC (DETMPC) [19–22], and periodic ETMPC [23, 24].

In DETMPC, the triggering threshold of the event-triggered mechanism is dynamically adjusted according to system requirements [19, 25]. Compared with conventional ETMPC utilizing static thresholds, DETMPC is capable of decreasing the triggering frequency due to this feature, thereby achieving a better trade-off between the

* Corresponding author (email: fengjw@szu.edu.cn, wangjingyi@szu.edu.cn)

computational efficiency and control performance [19]. Specifically, in [19], a DETMPC scheme was developed for the asynchronous coordination of linear MASs, which exhibited lower conservativeness for further lessening the unnecessary triggering instants. Liu et al. [26] introduced a dynamic triggering level to the interpolation-based MPC algorithm. Moreover, Shi et al. [20] proposed a DETMPC algorithm for Markovian jump systems subject to external disturbances. Nevertheless, these impressive results primarily concentrate on discrete-time systems. To the best of the authors' knowledge, limited research has addressed the design of DETMPC algorithms for continuous-time nonlinear MASs. This gap stems from the inherent challenge of simultaneously preventing Zeno behavior and formulating suitable triggering conditions to ensure system performance in DETMPC for continuous-time systems, which motivates the focus of this article.

Despite the effectiveness of the aforementioned event-based MPC algorithms in reducing computational resources, certain fast-response dynamic systems may still render them inapplicable. The main reason is that it is time-consuming and prohibitively expensive to activate the solver for the optimization problem at each update instant, which is another inevitable bottleneck for the MPC problem [27]. To address this challenge, an alternative approach is to implement a prediction horizon shrinkage strategy to alleviate the computational complexity of the optimization problem. The inspiration of the shrinkage mechanism is that the prediction horizon in MPC can be shortened appropriately as the system state approaches the terminal region [27–31]. This reduction effectively decreases the number of decision variables of the optimization problem, thereby enhancing computational efficiency. An adaptive prediction horizon scheme was incorporated into an event-triggered intermittent sampling algorithm in [29]. In [30, 31], the authors extended the results in [29] to the distributed control of MASs and the MASs with packet losses, respectively. More recently, in [27], a novel adaptive ETMPC algorithm with variable prediction horizons was proposed, providing a flexible approach for reducing the prediction horizon with an online shrinkage factor. However, only single-agent systems were considered in [27], which leaves room for further development. Inspired by the above, the development of an efficient DETMPC algorithm with a prediction horizon shrinkage strategy merits further investigation.

In this article, a novel DETMPC algorithm is proposed for the continuous-time nonlinear MASs. The main contributions are threefold.

(1) Unlike the schemes in [19–21, 27], a DETMPC algorithm is developed for the continuous-time nonlinear MASs with input constraints and additive disturbances. The triggering instants are generated only when the difference between the predicted state and the actual state exceeds a dynamic threshold, which is dynamically adjusted within an appropriately designed interval. As a result, compared with [16, 17], the proposed algorithm further reduces the frequency of solving the optimization problem to achieve a better balance between the computational efficiency and control performance.

(2) A prediction horizon shrinkage mechanism is designed for MASs, which effectively reduces the computational complexity of solving the optimization problem at each updated instant. In addition, compared with [16, 20, 21, 27], a robustness constraint, combined with the shrinkage strategy, is designed for the optimization problem to provide a decreasing upper bound for tightening the predicted state trajectory, thereby enhancing robustness against external disturbances and facilitating stability analysis of the proposed algorithm.

(3) The recursive feasibility of the overall algorithm and the robust stability of the resulting closed-loop system are thoroughly investigated, with sufficient conditions theoretically provided. Furthermore, the Zeno behavior of the dynamic event-triggered mechanism is eliminated.

The remainder of this article is organized as follows. The problem formulation is introduced in Section 2. The DETMPC algorithm that includes the optimization problem and the dynamic event-triggered mechanism is elaborated in Section 3. The detailed analysis of the proposed algorithm is illustrated in Section 4. Section 5 evaluates control performance through a numerical example and comparisons and Section 6 concludes this article.

Notations: Let $\mathbb{N}$ and $\mathbb{R}^n$ be the non-negative integers and the n-dimensional Euclidean space, respectively. For a given matrix $\mathcal{M}$, $\mathcal{M}^\top$ stands for its transpose. For a symmetric matrix $\mathcal{H}$, the notation $\mathcal{H} \succ 0$ indicates $\mathcal{H}$ is positive-definite. $\bar{\lambda}(\mathcal{H})$ (or $\underline{\lambda}(\mathcal{H})$) is the maximum (or minimum) eigenvalue of $\mathcal{H}$. Given a vector $\boldsymbol{x}$, we refer to $\|\boldsymbol{x}\| = \sqrt{\boldsymbol{x}^\top \boldsymbol{x}}$ as the 2-norm and $\|\boldsymbol{x}\|_{\mathcal{H}} = \sqrt{\boldsymbol{x}^\top \mathcal{H} \boldsymbol{x}}$ as the $\mathcal{H}$-weighted norm. Matrix dimensions are assumed to be compatible throughout this work.

2 Problem formulation

2.1 Graph theory

The network topological structure among N nonlinear agents is described as a directed graph $\mathscr{G} = \{\mathscr{V}, \mathscr{E}\}$, with a

vertex set $\mathscr{V} = \{1, 2, \cdots, N\}$ and an edge set $\mathscr{E} \subseteq \mathscr{V} \times \mathscr{V}$ included. An ordered pair $(j, i) \in \mathscr{E}$ indicates that the j-th agent can transmit information directly to the i-th agent, but not vice versa. Let $\mathscr{N}_i^{in} = \{j \in \mathscr{V} | (j, i) \in \mathscr{E}\}$ represent the set of in-neighbors for agent i. Similarly, let $\mathscr{N}_i^{out} = \{j \in \mathscr{V} | (i, j) \in \mathscr{E}\}$ be the out-neighbor set of agent i. Let $|\mathscr{N}_i^{in}|$ denote the cardinality of $\mathscr{N}_i^{in}$. The communication graph $\mathscr{G}$ is assumed to be fixed and connected to focus on the development of the DETMPC algorithm.

2.2 Agent dynamics

Consider the dynamics of agent i in MASs that is given by

$$\dot{\boldsymbol{x}}_i(t) = f_i(\boldsymbol{x}_i(t), \boldsymbol{u}_i(t)) + \boldsymbol{\omega}_i(t),\ \boldsymbol{x}_i(t_0) = \boldsymbol{x}_{i0},\ t \geqslant t_0, \tag{1}$$

where $\boldsymbol{x}_i(t) \in \mathbb{R}^n$ and $\boldsymbol{u}_i(t) \in \mathbb{R}^m$ are the system state and control input of agent i, respectively, and $\boldsymbol{\omega}_i(t) \in \mathbb{R}^n$ represents the external disturbance. Here, the control input $\boldsymbol{u}_i(t)$ and the disturbance $\boldsymbol{\omega}_i(t)$ belong to the following sets:

$$\boldsymbol{u}_i(t) \in \mathscr{U}_i,\ \boldsymbol{\omega}_i(t) \in \mathscr{W}_i,$$

where both $\mathscr{U}_i \subseteq \mathbb{R}^m$ and $\mathscr{W}_i \subseteq \mathbb{R}^n$ are compact convex sets with the origin as the interior point, and the disturbance admits an upper bound $\varrho_i \triangleq \sup_{\boldsymbol{\omega}_i(t) \in \mathscr{W}_i} \|\boldsymbol{\omega}_i(t)\|$. Also, the nominal system that corresponds to agent i in (1) is expressed as

$$\dot{\hat{\boldsymbol{x}}}_i(t) = f_i(\hat{\boldsymbol{x}}_i(t), \hat{\boldsymbol{u}}_i(t)). \tag{2}$$

Note that the i-th agent's system dynamics $f_i : \mathbb{R}^n \times \mathbb{R}^m \to \mathbb{R}^n$ with $f_i(0, 0) = 0$ is twice continuously differentiable and there exists a constant $L_i > 0$, $\forall \hat{\boldsymbol{x}}, \boldsymbol{x}, \boldsymbol{u}$ such that

$$||f_i(\hat{\boldsymbol{x}}, \boldsymbol{u}) - f_i(\boldsymbol{x}, \boldsymbol{u})||_{\mathcal{P}_i} \leqslant L_i ||\hat{\boldsymbol{x}} - \boldsymbol{x}||_{\mathcal{P}_i},$$

where $\mathcal{P}_i$ is the weighting matrix for agent i.

A state-feedback controller is employed to stabilize the closed-loop system within the terminal region, where the design of the feedback gain and the terminal region depends on the linearization of (2). Towards this objective, the i-th nominal linearized system around the origin is given as follows:

$$\dot{\hat{\boldsymbol{x}}}_i(t) = \mathcal{A}_i \hat{\boldsymbol{x}}_i(t) + \mathcal{B}_i \hat{\boldsymbol{u}}_i(t), \tag{3}$$

where $\mathcal{A}_i = (\partial f_i / \partial \hat{\boldsymbol{x}}_i)|_{(0,0)}$ and $\mathcal{B}_i = (\partial f_i / \partial \hat{\boldsymbol{u}}_i)|_{(0,0)}$. Next, a mild assumption on system (3) is provided, which facilitates the introduction of the following lemma.

Assumption 1 ([32]). The matrix pair $(\mathcal{A}_i, \mathcal{B}_i), i \in \mathscr{V}$, is stabilizable, that is, there exists a decentralized stability gain $\mathcal{K}_i$ such that $\mathcal{A}_i + \mathcal{B}_i \mathcal{K}_i$ is Hurwitz.

Afterwards, a well-known result on the control invariant property of the nonlinear model in (2) is presented as follows.

Lemma 1 ([32]). For system (2) with Assumption 1 and given matrices $\mathcal{R}_i \succ 0$ and $\mathcal{Q}_i \succ 0$, there exist a matrix $\mathcal{P}_i \succ 0$ and a constant $\varepsilon_i > 0$ such that the following.

(I) $\Psi_i(\varepsilon_i) \triangleq \{\hat{\boldsymbol{x}}_i(t) | V_i(\hat{\boldsymbol{x}}_i(t)) \leqslant \varepsilon_i^2\}$ is control invariant under the feedback controller $\hat{\boldsymbol{u}}_i(t) = \mathcal{K}_i \hat{\boldsymbol{x}}_i(t) \in \mathscr{U}_i$, where $V_i(\hat{\boldsymbol{x}}_i(t)) \triangleq \hat{\boldsymbol{x}}_i^\top(t) \mathcal{P}_i \hat{\boldsymbol{x}}_i(t)$.

(II) $\dot{V}_i(\hat{\boldsymbol{x}}_i(t)) \leqslant - \|\hat{\boldsymbol{x}}_i(t)\|_{\mathcal{Q}_i^*}^2$ holds for any $\hat{\boldsymbol{x}}_i(t) \in \Psi_i(\varepsilon_i)$, where $\mathcal{Q}_i^* \triangleq \mathcal{Q}_i + \mathcal{K}_i^\top \mathcal{R}_i \mathcal{K}_i$.

The goal of this article is to develop a DETMPC algorithm for each agent. The event-triggered strategy inherently prioritizes efficient resource reduction, even at the expense of some control performance. However, several results [19, 33] have shown that satisfactory control performance can be achieved despite reducing the triggering numbers. Therefore, the proposed algorithm aims to provide a better trade-off between computational efficiency and system performance compared to static ETMPC [16, 17]. Furthermore, the computational complexity of the optimization problem can be effectively reduced by designing a prediction horizon shrinkage strategy for each agent. These two aspects facilitate the efficient and economical utilization of computational resources in the proposed algorithm.

3 Dynamic event-triggered MPC

In this section, we first formulate the optimization problem for each agent, followed by the design of the dynamic event-triggered mechanism. The overall algorithm is then presented at the end of the section.

3.1 Optimization problem

Before proceeding to the design of the optimization problem, several notations are introduced. Let $\{t_p\}_{p\in\mathbb{N}}$ denote the triggering time sequence at which the optimization problem is solved, and each agent transmits the corresponding system information to its out-neighbors. The prediction horizon is denoted by H_p, which varies with t_p and will be developed subsequently. To formulate the optimization problem, the cost function at t_p for agent i is defined as

$$\begin{aligned}\boldsymbol{J}_i(\hat{\boldsymbol{x}}_i(\tau|t_p),\tilde{X}_i(\tau|t_p),\hat{\boldsymbol{u}}_i(\tau|t_p)) \triangleq \int_{t_p}^{t_p+H_p}\Bigg(&\|\hat{\boldsymbol{x}}_i(\tau|t_p)\|_{\mathcal{Q}_i}^2+\|\hat{\boldsymbol{u}}_i(\tau|t_p)\|_{\mathcal{R}_i}^2\\&+\sum_{j\in\mathscr{N}_i^{in}}\|\hat{\boldsymbol{x}}_i(\tau|t_p)-\tilde{\boldsymbol{x}}_j(\tau|t_p)\|_{\mathcal{Q}_{ij}}^2\Bigg)\mathrm{d}\tau+\|\hat{\boldsymbol{x}}_i(t_p+H_p|t_p)\|_{\mathcal{P}_i}^2,\end{aligned}$$

where $\mathcal{Q}_i$, $\mathcal{R}_i$ and $\mathcal{P}_i$ are weighting matrices according to Lemma 1, and $\mathcal{Q}_{ij}\succ 0$ represents the cooperation matrix between agent i and agent j. On the time interval $\tau\in[t_p,t_p+H_p]$, $\hat{\boldsymbol{x}}_i(\tau|t_p)$ and $\hat{\boldsymbol{u}}_i(\tau|t_p)$ denote the predicted state and control trajectories, respectively, which satisfy $\dot{\hat{\boldsymbol{x}}}_i(\tau|t_p)=f_i(\hat{\boldsymbol{x}}_i(\tau|t_p),\hat{\boldsymbol{u}}_i(\tau|t_p))$. With $\hat{\boldsymbol{u}}_i^*(\tau|t_p)$ being the optimal control input, the optimal state trajectory is denoted by $\hat{\boldsymbol{x}}_i^*(\tau|t_p)$ accordingly. $\tilde{X}_i=\{\tilde{\boldsymbol{x}}_{i1},\cdots,\tilde{\boldsymbol{x}}_{i|\mathscr{N}_i^{in}|}\}$ is constituted by the neighboring assumed state trajectory for the i-th agent, where $\tilde{\boldsymbol{x}}_j(\tau|t_p)$, $j\in\mathscr{N}_i^{in}$, is generated as

$$\begin{cases}\tilde{\boldsymbol{x}}_j(\tau|t_p)=\hat{\boldsymbol{x}}_j^*(\tau|t_{p-1}),\quad \tau\in[t_p,t_{p-1}+H_{p-1}],\\ \dot{\tilde{\boldsymbol{x}}}_j(\tau|t_p)=f_j(\tilde{\boldsymbol{x}}_j(\tau|t_p),\mathcal{K}_j\tilde{\boldsymbol{x}}_j(\tau|t_p)),\tau\in(t_{p-1}+H_{p-1},t_p+H_p].\end{cases}\tag{4}$$

Remark 1. Within the cost function, the terms $\|\hat{\boldsymbol{x}}_i(\tau|t_p)\|_{\mathcal{Q}_i}^2$ and $\|\hat{\boldsymbol{u}}_i(\tau|t_p)\|_{\mathcal{R}_i}^2$ represent the stage costs associated with the state and control input, respectively, weighted by the matrices $\mathcal{Q}_i$ and $\mathcal{R}_i$. The terminal cost $\|\hat{\boldsymbol{x}}_i(t_p+H_p|t_p)\|_{\mathcal{P}_i}^2$ is crucial for the stability analysis. Given $\mathcal{Q}_i$ and $\mathcal{R}_i$, the matrix $\mathcal{P}_i$ can be derived by using the Lyapunov equation. Moreover, motivated by [19, 23, 32], the term $\sum_{j\in\mathscr{N}_i^{in}}\|\hat{\boldsymbol{x}}_i(\tau|t_p)-\tilde{\boldsymbol{x}}_j(\tau|t_p)\|_{\mathcal{Q}_{ij}}^2\mathrm{d}\tau$ in the cost function is utilized to coordinate the agents of MASs. By minimizing the difference of this term between agent i and its neighboring agents, the overall state of MASs can be synchronized as closely as possible.

In what follows, in order to derive the optimal control trajectory $\hat{\boldsymbol{u}}_i^*(\tau|t_p)$ for $\tau\in[t_p,t_p+H_p]$, agent i solves the following optimization problem $\mathscr{P}_i$ at the triggering instant t_p:

$$\begin{aligned}&\hat{\boldsymbol{u}}_i^*(\tau|t_p)=\arg\min_{\hat{\boldsymbol{u}}_i(\tau|t_p)}\boldsymbol{J}_i(\hat{\boldsymbol{x}}_i(\tau|t_p),\tilde{X}_i(\tau|t_p),\hat{\boldsymbol{u}}_i(\tau|t_p))\\ \text{s.t.}\quad&\dot{\hat{\boldsymbol{x}}}_i(\tau|t_p)=f_i(\hat{\boldsymbol{x}}_i(\tau|t_p),\hat{\boldsymbol{u}}_i(\tau|t_p)),\tau\in[t_p,t_p+H_p],\\&\hat{\boldsymbol{x}}_i(t_p|t_p)=\boldsymbol{x}_i(t_p),\\&\hat{\boldsymbol{u}}_i(\tau|t_p)\in\mathscr{U}_i,\tau\in[t_p,t_p+H_p],\\&\|\hat{\boldsymbol{x}}_i(\tau|t_p)\|_{\mathcal{P}_i}\leqslant\frac{\alpha_i H_p}{\tau-t_p}\boldsymbol{\varepsilon}_i,\tau\in(t_p,t_p+H_p],\end{aligned}\tag{5}$$

where $\alpha_i\in(0,1)$ is the scaling parameter of (5) for the i-th agent. By defining H_{ip}^* as the time interval when $\hat{\boldsymbol{x}}_i^*(t_p+H_{ip}^*|t_p)$ reaches the boundary of $\Psi_i(\alpha_i\boldsymbol{\varepsilon}_i)$, the prediction horizon for each agent evolves as

$$H_{p+1}=H_p-\mu_p(H_p-H_p^*),\tag{6}$$

where $H_p^*=\max_{i\in\mathscr{V}}\{H_{ip}^*\}$, and $\mu_p>0$ denotes the shrinkage factor of the prediction horizon. Notice that the selection of the initial prediction horizon H_0 needs to guarantee that $\mathscr{P}_i$ is initially feasible, which is fundamental for the feasibility and stability analysis. Hence, the following assumption is made.

Assumption 2 ([32, 34])**.** The optimization problem $\mathscr{P}_i$ is feasible for the initial prediction horizon H_0, $i\in\mathscr{V}$.

Remark 2. The innovation of the optimization problem $\mathscr{P}_i$ is that we utilize a $\mathcal{P}_i$-weighted norm constraint (5), called the robustness constraint, to confine the predicted state trajectory $\hat{\boldsymbol{x}}_i(\tau|t_p)$ on the time interval $\tau\in[t_p,t_p+H_p]$. When $\tau=t_p+H_p$, this constraint serves as the terminal constraint in conventional MPC, indicating $\hat{\boldsymbol{x}}_i(t_p+H_p|t_p)\in\Psi_i(\alpha_i\boldsymbol{\varepsilon}_i)$. Furthermore, since the cost function serves as a Lyapunov function in the stability analysis, the constraint (5) on the predicted states helps ensure its monotonic decrease over time. If $H_p\equiv H,\forall p\in\mathbb{N}$ with H as a positive constant, then Eq. (5) becomes the robustness constraint with the static prediction horizon in [16, 32]. Consequently, Eq. (5) provides a more general formulation than the tightening constraints in [16, 32].

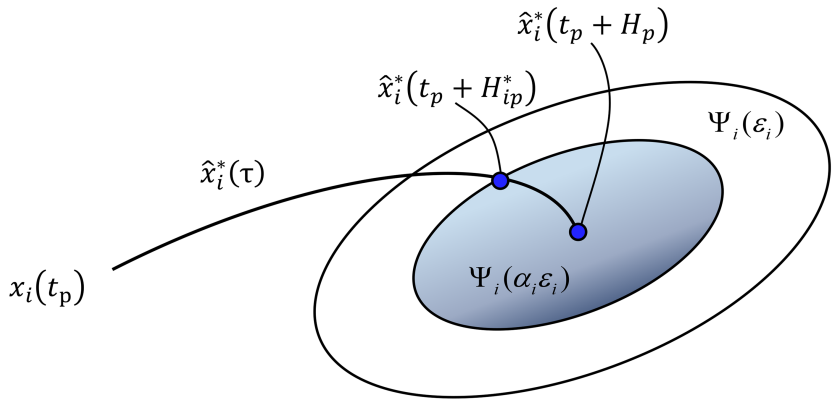

Figure 1 (Color online) Graphical description of the relationship between the optimal state trajectory and two terminal regions.

Moreover, most MPC algorithms with the prediction horizon shrinkage scheme encounter challenges when it comes to formulating an optimization problem with the robustness constraint (5), which distinguishes our work from previous studies [29–31].

Remark 3. At the updated instant t_p, due to the terminal constraint $\hat{\boldsymbol{x}}_i(t_p + H_p|t_p) \in \Psi_i(\alpha_i\boldsymbol{\varepsilon}_i)$ by (5), H_{ip}^* can be obtained by solving the optimization problem $\mathscr{P}_i$ online for the i-th agent (A schematic diagram in Figure 1 illustrates this design). The prediction horizon is then updated according to (6) with H_{ip}^* and an appropriate value of μ_p. Particularly, μ_p will be determined from the established conditions for the recursive feasibility and closed-loop stability. It should be noted that the prediction horizon H_p is monotonically decreasing due to the update scheme in (6). In this aspect, compared with the fixed prediction horizon [16, 17, 32], the optimization problem $\mathscr{P}_i$ with the robustness constraint (5) enjoys lower computational complexity, thereby reducing the computational resources. In addition, a larger value of μ_p leads to a faster reduction in computational complexity and system convergence compared to a smaller value μ_p. Therefore, the update rule in (6) achieves a more favorable trade-off between the control performance and resource consumption compared with the shrinkage schemes in [29–31].

3.2 Dynamic event-triggered strategy

Following the preceding MPC problem, a novel event-triggered mechanism is developed to determine the triggering instant t_p. Owing to the ubiquitous existence of the disturbances, the actual state trajectory $\boldsymbol{x}_i(\tau)$ will diverge from its optimal state trajectory $\hat{\boldsymbol{x}}_i^*(\tau|t_p)$ during the time interval $\tau \in [t_p, t_p + H_p]$. To confine this deviation and adjust the frequency of solving the optimization problem $\mathscr{P}_i$, an event-triggered generator function with a time variable $\eta_i(\tau)$ for the i-th agent is defined as

$$\tilde{t}_{p+1}^i = \inf_{\tau > t_p} \{\tau : ||\boldsymbol{x}_i(\tau) - \hat{\boldsymbol{x}}_i^*(\tau|t_p)||_{\mathcal{P}_i} = \eta_i(\tau)\}. \tag{7}$$

The description of the time variable $\eta_i(\tau)$ for $\tau \in (t_p, t_{p+1}]$ is that if $\eta_i(\tau) < \eta_{ip}^{\max}$, then

$$\dot{\eta}_i(\tau) = -a_i\eta_i(\tau) - b_i \left\|\boldsymbol{x}_i(\tau) - \hat{\boldsymbol{x}}_i^*(\tau|t_p)\right\|_{P_i} + \eta_{ip}^{\min},$$

and otherwise $\dot{\eta}_i(\tau) = 0$, where $a_i + b_i = 1$, a_i and b_i are adjustable positive parameters and the lower bound $\eta_{ip}^{\min}$ and the upper bound $\eta_{ip}^{\max}$ of $\eta_i(\tau)$ are designed as

$$\begin{aligned} \eta_{ip}^{\min} &= \varrho_i\beta H_p\bar{\lambda}(\sqrt{\mathcal{P}_i})e^{\beta H_p L_i}, \\ \eta_{ip}^{\max} &= (1-\alpha_i)\boldsymbol{\varepsilon}_i e^{-(1-\beta)H_p L_i}, \end{aligned} \tag{8}$$

where $\beta \in (0, 1)$ is a tunable constant. Under the time instant $\tilde{t}_{p+1}^i$ by (7), the triggering instant t_{p+1} is generated as

$$t_{p+1} = \min\{\tilde{t}_{p+1}^1, \cdots, \tilde{t}_{p+1}^N, t_p + H_p\}, \tag{9}$$

thereby the resultant triggering time sequence $\{t_p\}_{p\in\mathbb{N}}$ completes the optimization problem $\mathscr{P}_i$.

Remark 4. In (7), $\eta_i(\tau)$ is a dynamic variable but not monotonically decreasing, where the update rule involves a negative self-feedback term, the deviation error, and the lower bound of the triggering threshold. The requirement

$a_i + b_i = 1$ is imposed to ensure that $\eta_i(\tau) \in [\eta_{ip}^{\min}, \eta_{ip}^{\max}]$ always holds on the time interval $\tau \in [t_p, t_p + H_p]$, which will be detailed in Lemma 2. Moreover, the lower bound designed in (8) is the same as the fixed triggering threshold in [16], while its upper bound contributes to the analysis of Lemma 3 and recursive feasibility. If $\dot{\eta}_i(\tau) \equiv 0$ and $\eta_i(t_0) \neq 0$, then Eq. (7) becomes the static event-triggered condition in [16]. Thereafter, Proposition 1 will provide a theoretical analysis comparing the resource consumption of (9) with the traditional event-triggered strategy.

Lemma 2. For agent (1) under the dynamic event-triggered strategy (9) with the triggering parameters (8), if $\varrho_i \leqslant \frac{(1-\alpha_i)\boldsymbol{\varepsilon}_i e^{-H_0 L_i}}{\beta H_0 \bar{\lambda}(\sqrt{\mathcal{P}_i})}$ and $\eta_i(t_0) \in [\eta_{i0}^{\min}, \eta_{i0}^{\max}]$, then $\eta_{ip}^{\min} \leqslant \eta_{ip}^{\max}$ and $\eta_i(\tau) \in [\eta_{ip}^{\min}, \eta_{ip}^{\max}]$ are satisfied on the time interval $\tau \in (t_p, t_{p+1}]$ for any $p \in \mathbb{N}$.

Proof. It is noteworthy that $\eta_{ip}^{\max}$ and $\eta_{ip}^{\min}$ in (8) are monotonically increasing and decreasing, respectively, because the prediction horizon H_p becomes smaller under the shrinking strategy in (6). Therefore, in order to ensure $\eta_{ip}^{\min} \leqslant \eta_{ip}^{\max}$ for any $p \in \mathbb{N}$, it suffices to prove $\eta_{i0}^{\min} \leqslant \eta_{i0}^{\max}$ at the initial prediction horizon H_0, which is ensured by the condition $\varrho_i \leqslant \frac{(1-\alpha_i)\boldsymbol{\varepsilon}_i e^{-H_0 L_i}}{\beta H_0 \bar{\lambda}(\sqrt{\mathcal{P}_i})}$.

Next, recalling the design of $\dot{\eta}_i(\tau)$ and the condition $\eta_i(t_0) \leqslant \eta_{i0}^{\max}$, it directly yields $\eta_i(\tau) \leqslant \eta_{ip}^{\max}$, $\tau \in (t_p, t_{p+1}]$. To prove $\eta_i(\tau) \geqslant \eta_{ip}^{\min}$, on one hand, suppose that there exists a time instant $\bar{t}_p \in (t_p, t_{p+1}]$ such that $\eta_i(\bar{t}_p) = \eta_{ip}^{\max}$. Thus, in the time interval $\tau \in (t_p, \bar{t}_p)$, it holds

$$\dot{\eta}_i(\tau) = -a_i \eta_i(\tau) - b_i \left\| \boldsymbol{x}_i(\tau) - \hat{\boldsymbol{x}}_i^*(\tau|t_p) \right\|_{\mathcal{P}_i} + \eta_{ip}^{\min}.$$

Meanwhile, no event is triggered in $(t_p, \bar{t}_p)$. Then one gets

$$||\boldsymbol{x}_i(\tau) - \hat{\boldsymbol{x}}_i^*(\tau|t_p)||_{\mathcal{P}_i} < \eta_i(\tau).$$

Following the above results, we obtain

$$\dot{\eta}_i(\tau) > -(a_i + b_i)\left(\eta_i(\tau) - \eta_{ip}^{\min}\right),$$

which further implies

$$\eta_i(\tau) > \left(\eta_i(t_p) - \eta_{ip}^{\min}\right) e^{-(\tau - t_p)} + \eta_{ip}^{\min},\ \tau \in (t_p, \bar{t}_p]. \tag{10}$$

Specifically, substituting $\tau = \bar{t}_p$ into (10), we have

$$\eta_i(\bar{t}_p) > \left(\eta_i(t_p) - \eta_{ip}^{\min}\right) e^{-(\bar{t}_p - t_p)} + \eta_{ip}^{\min}.$$

From the definition of $\dot{\eta}_i(\tau)$ for $\tau \in [\bar{t}_p, t_{p+1}]$, one derives

$$\begin{aligned} \eta_i(\tau) =& \eta_i(\bar{t}_p) \\ >& \left(\eta_i(t_p) - \eta_{ip}^{\min}\right) e^{-(\tau - t_p)} + \eta_{ip}^{\min}. \end{aligned}$$

On the other hand, if $\eta_i(\tau) < \eta_{ip}^{\max}$ for $\tau \in (t_p, t_{p+1}]$, one has

$$\eta_i(\tau) \geqslant \left(\eta_i(t_p) - \eta_{ip}^{\min}\right) e^{-(\tau - t_p)} + \eta_{ip}^{\min}. \tag{11}$$

Since the analysis procedure of (11) is analogous to (10), we omit here for a simplified description. As a result, when $\tau \in (t_p, t_{p+1}]$, it can be concluded that the inequality in (11) always holds. By induction, we further obtain

$$\begin{aligned} \eta_i(\tau) \geqslant& \left[(\eta_i(t_{p-1}) - \eta_{i(p-1)}^{\min}) e^{-(t_p - t_{p-1})} + \eta_{i(p-1)}^{\min} - \eta_{ip}^{\min}\right] e^{-(\tau - t_p)} + \eta_{ip}^{\min} \\ \geqslant& \left(\eta_i(t_{p-1}) - \eta_{i(p-1)}^{\min}\right) e^{-(\tau - t_{p-1})} + \eta_{ip}^{\min} \\ &\vdots \\ \geqslant& \left(\eta_i(t_0) - \eta_{i0}^{\min}\right) e^{-(\tau - t_0)} + \eta_{ip}^{\min} \\ \geqslant& \eta_{ip}^{\min}, \end{aligned}$$

where the second inequality is ensured by the decreasing property of $\eta_{ip}^{\min}$, and the last inequality is straightforward from the condition in Lemma 2.

Proposition 1. For agent (1), implementing the dynamic event-triggered scheme (7) will lead to a larger inter-execution interval than the static case with $\eta_{ip}^{\min}$.

Proof. Given a triggering instant t_p, the following update instants are denoted by t_{p+1} and $\bar{t}_{p+1}$ when using the dynamic event-triggered scheme (7) and static one with $\eta_{ip}^{\min}$, respectively. By assuming $t_{p+1} < \bar{t}_{p+1}$, it follows that $t_{p+1} \in (t_p, \bar{t}_{p+1})$ and $||\boldsymbol{x}_i(t_{p+1}) - \hat{\boldsymbol{x}}_i^*(t_{p+1}|t_p)||_{\mathcal{P}_i} < \eta_{ip}^{\min}$. Nevertheless, in light of the triggering condition (7) at t_{p+1}, there exists $||\boldsymbol{x}_i(t_{p+1}) - \hat{\boldsymbol{x}}_i^*(t_{p+1}|t_p)||_{\mathcal{P}_i} = \eta_i(t_{p+1}) \geqslant \eta_{ip}^{\min}$, which contradicts the former inequality. As a result, we have $\bar{t}_{p+1} \leqslant t_{p+1}$.

Remark 5. According to Proposition 1, the dynamic event-triggered strategy (9) leads to an increased inter-execution interval, thereby reducing the utilization of computational resources compared with the static event-triggered strategies in [16, 17].

As a further matter, Zeno behavior is the occurrence of infinitely fast execution of events within a finite interval, which is unfavorable to the normal operation of the plant in the real world. In what follows, an analysis of a minimum time interval for the proposed dynamic event-triggered mechanism is presented.

Theorem 1. For agent (1) under the dynamic event-triggered strategy (9) with the triggering parameters (8), the minimum inter-event time satisfies $\inf_{p\in\mathbb{N}}\{t_{p+1} - t_p\} \geqslant \beta H_p$ and the maximum inter-event time satisfies $\sup_{p\in\mathbb{N}}\{t_{p+1} - t_p\} \leqslant H_p$.

Proof. The maximum inter-event time directly follows from the generator of t_{p+1}. In light of Lemma 2, we only need to estimate the minimum time interval under the triggering threshold $\eta_{ip}^{\min}$ for the elimination of the Zeno phenomenon. During the time interval $\tau \in (t_p, t_{p+1}]$, we take the dynamics of $\boldsymbol{x}_i(\tau)$ and $\hat{\boldsymbol{x}}_i^*(\tau|t_p)$ into account. Applying the triangle inequality and the Lipschitz condition, one gets

$$||\boldsymbol{x}_i(\tau) - \hat{\boldsymbol{x}}_i^*(\tau|t_p)||_{\mathcal{P}_i} \leqslant \int_{t_p}^{\tau} \left(L_i||\boldsymbol{x}_i(\xi) - \hat{\boldsymbol{x}}_i^*(\xi|t_p)||_{\mathcal{P}_i} + \varrho_i\bar{\lambda}(\sqrt{\mathcal{P}_i}) \right) \mathrm{d}\xi.$$

Utilizing the Gronwall-Bellman inequality, one has

$$||\boldsymbol{x}_i(\tau) - \hat{\boldsymbol{x}}_i^*(\tau|t_p)||_{\mathcal{P}_i} \leqslant \varrho_i(\tau - t_p)\bar{\lambda}(\sqrt{\mathcal{P}_i})e^{(\tau-t_p)L_i}. \tag{12}$$

By combining $||\boldsymbol{x}_i(\tau) - \hat{\boldsymbol{x}}_i^*(\tau|t_p)||_{\mathcal{P}_i} \leqslant \eta_{ip}^{\min}$ and (12), one has $\inf_{k\in\mathbb{N}}\{t_{p+1} - t_p\} \geqslant \beta H_p$ holds.

Remark 6. Since H_p decreases monotonically, so does the interval βH_p in Theorem 1. However, $H_p > 0$ is guaranteed by the adopted dual-mode framework throughout the MPC phase (i.e., $\boldsymbol{x}_i(t) \notin \Psi_i(\boldsymbol{\varepsilon}_i)$), and is further theoretically ensured by the analysis provided in Remark 8. Thereby, the proposed mechanism maintains a strictly positive minimum triggering interval $\beta H_p > 0$, thereby excluding Zeno behavior.

3.3 Dynamic event-triggered MPC algorithm for MASs

By integrating the optimization problem $\mathscr{P}_i$ with the dynamic event-triggered strategy, we adopt the dual-mode control scheme in [16] for each agent as well to effectively reduce the communication and computational resources. Simply put, if the state of the i-th agent is inside the region $\Psi_i(\boldsymbol{\varepsilon}_i)$, the local feedback controller $\boldsymbol{u}_i(t) = \mathcal{K}_i\boldsymbol{x}_i(t)$ is applied to agent i; otherwise, the optimal control input $\hat{\boldsymbol{u}}_i^*(\tau|t_p)$ from the optimization problem $\mathscr{P}_i$ is applied. For a clear view of the algorithm execution, the overall algorithm is divided into two parts. Specifically, the offline part, denoted by Algorithm 1, focuses on the selection of system parameters. By combining the sufficient conditions established in Section 4, Algorithm 1 outlines how to start the control procedure with the appropriate parameters. Meanwhile, the online part of the DETMPC algorithm for MASs is dedicated to generating control input trajectories, which is summarized in Algorithm 2.

Algorithm 1 DETMPC algorithm: offline part.

1: Input weighting matrices $\mathcal{Q}_i, \mathcal{R}_i, \mathcal{Q}_{ij}$ and utilize the LQR approach to derive the matrix $\mathcal{P}_i$ and the feedback gain $\mathcal{K}_i$;
2: Input function f_i and calculate L_i by virtue of Lemma 3.2 and Lemma 3.3 in [35];
3: According to [36], construct the terminal region $\Psi_i(\boldsymbol{\varepsilon}_i)$;
4: Select H_0 according to Assumption 2; set α_i, β and determine the permissible disturbance ϱ_i based on Lemma 2 and Theorem 3;
5: Set the initial triggering threshold η_{i0} and tunable parameters a_i, b_i.

Remark 7. In order to achieve real-time transmission between agents, a synchronous update mechanism is considered to deal with the theoretical challenge under the shrinkage strategy of the prediction horizon. Admittedly, the asynchronous update strategy has lower resource consumption in the sense that it divides decision-making among agents and only uses partial information, which will be our future focus.

Algorithm 2 DETMPC algorithm: online part.

Initialization: For agent i, set $p=0$, t_0, $\boldsymbol{x}_{i0}$; determine the control parameters according to Algorithm 1; each agent transmits the initial state to the agents belonging to $\mathscr{N}_i^{out}$;
1: **while** $\boldsymbol{x}_i(t) \notin \Psi_i(\boldsymbol{\varepsilon}_i)$ **do**
2: **if** p=0 or t_p is triggered **then**
3: Calculate the assumed state trajectory $\tilde{\boldsymbol{x}}_j(\tau|t_p)$ for $\tau \in [t_p, t_p+H_p]$ by (4);
4: Solve the optimization problem $\mathscr{P}_i$ to obtain $\hat{\boldsymbol{x}}_i^*(\tau|t_p)$, $\hat{\boldsymbol{u}}_i^*(\tau|t_p)$, $\tau \in [t_p, t_p+H_p]$, H_{ip}^*, and send out $\hat{\boldsymbol{x}}_i^*(\tau|t_p), H_{ip}^*$ through the communication network $\mathscr{G}$;
5: Update the triggering parameters $\eta_{ip}^{\min}$ and $\eta_{ip}^{\max}$ according to (8);
6: Determine μ_p according to the conditions in (14), (17), (18) and (24); if μ_p is not obtained, activate Algorithm 1 and return to Step 4;
7: Set $p=p+1$;
8: Update the prediction horizon H_p according to (6);
9: **end if**
10: Apply $\hat{\boldsymbol{u}}_i^*(\tau|t_{p-1})$ for $\tau \in [t_{p-1}, t_{p-1}+H_{p-1}]$ to agent i;
11: Calculate $\eta_i(t)$ according to (7);
12: **end while**
13: Apply the local feedback controller $\boldsymbol{u}_i(t)=\mathcal{K}_i\boldsymbol{x}_i(t)$.

4 Analysis

4.1 Feasibility analysis

This subsection analyzes the recursive feasibility, indicating that if the current optimization problem $\mathscr{P}_i$ has an optimal solution, then the next updated instant will also yield a feasible solution. To this end, provided that the optimization problem $\mathscr{P}_i$ is feasible at t_p and the corresponding optimal control trajectory is given by $\hat{\boldsymbol{u}}_i^*(\tau|t_p)$, $\tau \in [t_p, t_p+H_p]$, a feasible control candidate $\hat{\boldsymbol{u}}_i^o(\tau|t_{p+1})$ is designed at t_{p+1}, which is of the setup

$$\hat{\boldsymbol{u}}_i^o(\tau|t_{p+1}) = \begin{cases} \hat{\boldsymbol{u}}_i^*(\tau|t_p), & \tau \in [t_{p+1}, t_p+H_p], \\ \mathcal{K}_i\hat{\boldsymbol{x}}_i^o(\tau|t_{p+1}), & \tau \in (t_p+H_p, t_{p+1}+H_{p+1}], \end{cases} \tag{13}$$

where $\hat{\boldsymbol{x}}_i^o(\tau|t_{p+1})$ is the feasible state candidate satisfying $\dot{\hat{\boldsymbol{x}}}_i^o(\tau|t_{p+1}) = f_i(\hat{\boldsymbol{x}}_i^o(\tau|t_{p+1}), \hat{\boldsymbol{u}}_i^o(\tau|t_{p+1}))$ with the initial value $\boldsymbol{x}_i(t_{p+1})$. We first present a lemma to demonstrate that the state trajectory $\hat{\boldsymbol{x}}_i^o(\tau|t_{p+1})$ of agent i will be steered into the $\Psi_i(\alpha_i\boldsymbol{\varepsilon}_i)$ if certain conditions are satisfied.

Lemma 3. Suppose Assumptions 1 and 2 hold. For the i-th agent with feasible control candidate (13), if the optimization problem $\mathscr{P}_i$ is feasible at t_p and satisfies

$$\mu_p \leqslant \frac{2\bar{\lambda}(\mathcal{P}_i)\ln\alpha_i + \beta H_p \underline{\lambda}(\mathcal{Q}_i^*)}{\underline{\lambda}(\mathcal{Q}_i^*)(H_p - H_p^*)}, \tag{14}$$

then $\hat{\boldsymbol{x}}_i^o(t_{p+1}+H_{p+1}|t_{p+1}) \in \Psi_i(\alpha_i\boldsymbol{\varepsilon}_i)$.

Proof. When $\tau \in [t_{p+1}, t_p+H_p]$, considering the difference between $\hat{\boldsymbol{x}}_i^o(\tau|t_{p+1})$ and $\hat{\boldsymbol{x}}_i^*(\tau|t_p)$, one obtains

$$\begin{aligned} &\|\hat{\boldsymbol{x}}_i^o(\tau|t_{p+1}) - \hat{\boldsymbol{x}}_i^*(\tau|t_p)\|_{\mathcal{P}_i} \\ &= \|\hat{\boldsymbol{x}}_i^o(t_{p+1}|t_{p+1}) + \int_{t_{p+1}}^{\tau} f_i(\hat{\boldsymbol{x}}_i^o(\xi|t_{p+1}), \hat{\boldsymbol{u}}_i^o(\xi|t_{p+1}))\mathrm{d}\xi \\ &\quad - \hat{\boldsymbol{x}}_i^*(t_{p+1}|t_p) - \int_{t_{p+1}}^{\tau} f_i(\hat{\boldsymbol{x}}_i^*(\xi|t_p), \hat{\boldsymbol{u}}_i^*(\xi|t_p))\mathrm{d}\xi \ \|_{\mathcal{P}_i} \\ &\leqslant \eta_i(t_{p+1}) + \int_{t_{p+1}}^{\tau} L_i \|\hat{\boldsymbol{x}}_i^o(\xi|t_{p+1}) - \hat{\boldsymbol{x}}_i^*(\xi|t_p)\|_{\mathcal{P}_i}\mathrm{d}\xi, \end{aligned}$$

where the triggering condition in (7) has been utilized. By means of the Gronwall-Bellman inequality, one gets

$$\|\hat{\boldsymbol{x}}_i^o(\tau|t_{p+1}) - \hat{\boldsymbol{x}}_i^*(\tau|t_p)\|_{\mathcal{P}_i} \leqslant \eta_i(t_{p+1})e^{L_i(\tau-t_{p+1})}. \tag{15}$$

Afterwards, substituting $\tau = t_p+H_p$ into (15) and using the definition of $\eta_{ip}^{\max}$ in (8), one can find that

$$\begin{aligned} \|\hat{\boldsymbol{x}}_i^o(t_p+H_p|t_{p+1})\|_{\mathcal{P}_i} &\leqslant \|\hat{\boldsymbol{x}}_i^*(t_p+H_p|t_p)\|_{\mathcal{P}_i} + \eta_i(t_{p+1})e^{L_i(t_p+H_p-t_{p+1})} \\ &\leqslant \alpha_i\boldsymbol{\varepsilon}_i + \eta_{ip}^{\max}e^{(1-\beta)H_pL_i} \end{aligned}$$

$$=\boldsymbol{\varepsilon}_i,$$

which indicates $\hat{\boldsymbol{x}}_i^o(t_p+H_p|t_{p+1}) \in \Psi_i(\boldsymbol{\varepsilon}_i)$. As a result, Lemma 1 is valid and we derive $\dot{V}_i(\hat{\boldsymbol{x}}_i^o(\tau|t_{p+1})) \leqslant -\|\hat{\boldsymbol{x}}_i^o(\tau|t_{p+1})\|_{Q_i^*}^2$ for $\tau \in [t_p+H_p, t_{p+1}+H_{p+1}]$. Employing the comparison principle, one has

$$V_i(\hat{\boldsymbol{x}}_i^o(\tau|t_{p+1})) \leqslant \boldsymbol{\varepsilon}_i^2 e^{-\frac{\underline{\lambda}(\mathcal{Q}_i^*)}{\bar{\lambda}(\mathcal{P}_i)}(\tau-t_p-H_p)}. \tag{16}$$

With the minimum inter-event time and the update rule (6) in mind, letting $\tau = t_{p+1}+H_{p+1}$, it holds from (16) that

$$V_i(\hat{\boldsymbol{x}}_i^o(t_{p+1}+H_{p+1}|t_{p+1})) \leqslant \boldsymbol{\varepsilon}_i^2 e^{-\frac{\underline{\lambda}(\mathcal{Q}_i^*)}{\bar{\lambda}(\mathcal{P}_i)}\left(\beta H_p-\mu_p(H_p-H_p^*)\right)}.$$

Then, recalling the condition (14) in Lemma 3, one has $V_i(\hat{\boldsymbol{x}}_i^o(t_{p+1}+H_{p+1}|t_{p+1})) \leqslant \alpha_i^2\boldsymbol{\varepsilon}_i^2$, so the result $\hat{\boldsymbol{x}}_i^o(t_{p+1}+H_{p+1}|t_{p+1}) \in \Psi_i(\alpha_i\boldsymbol{\varepsilon}_i)$ can be derived.

Remark 8. By substituting (14) into (6), one derives $(1-\beta)H_p < H_{p+1}$. This implies that, with an appropriate initial prediction horizon $H_0 > 0$, $H_p > 0$ holds for any $p \in \mathbb{N}$, ensuring the rationality of the shrinking strategy in (6) and the positive minimum inter-event time $\beta H_p > 0$. In addition, since $\beta H_p \leqslant t_{p+1}-t_p$, we have $t_p+H_p \leqslant t_{p+1}+H_{p+1}$, which is essential for the interval division in Lemma 3.

With the aid of Lemma 3, Theorem 2 will demonstrate that the candidate trajectories $\hat{\boldsymbol{x}}_i^o(\tau|t_{p+1})$ and $\hat{\boldsymbol{u}}_i^o(\tau|t_{p+1})$ fulfill the constraints in the optimization problem $\mathscr{P}_i$ for $\tau \in [t_{p+1}, t_{p+1}+H_{p+1}]$.

Theorem 2. Suppose Assumptions 1 and 2 and the condition (14) hold. For the i-th agent, if the following inequalities:

$$\mu_p \leqslant \frac{(\alpha_i+\beta-1)H_p}{\alpha_i\left(H_p-H_p^*\right)} \tag{17}$$

and

$$H_{p+1}e^{\frac{\underline{\lambda}(\mathcal{Q}_i^*)}{2\bar{\lambda}(\mathcal{P}_i)}H_{p+1}} \leqslant \frac{2\bar{\lambda}(\mathcal{P}_i)}{\alpha_i\underline{\lambda}(\mathcal{Q}_i^*)} \tag{18}$$

are satisfied, then the DETMPC algorithm with the control sequence (13) is recursively feasible.

Proof. We utilize the induction principle to prove the recursive feasibility. Specifically, an initial feasible solution of the optimization problem $\mathscr{P}_i$ is guaranteed by Assumption 1. Then, for an expository reason, the proof procedure of the feasibility at t_{p+1} is divided into two aspects during the time interval $\tau \in [t_{p+1}, t_{p+1}+H_{p+1}]$: (i) $\|\hat{\boldsymbol{x}}_i^o(\tau|t_{p+1})\|_{\mathcal{P}_i} \leqslant \frac{\alpha_i H_{p+1}}{\tau-t_{p+1}}\boldsymbol{\varepsilon}_i$; (ii) $\hat{\boldsymbol{u}}_i^o(\tau|t_{p+1}) \in \mathscr{U}_i$.

First, take the dynamics of the state trajectory $\hat{\boldsymbol{x}}_i^o(\tau|t_{p+1})$ for $\tau \in [t_{p+1}, t_p+H_p]$ into consideration. By the designed constraint in (5) and triggering level (8), it holds from inequality (15) that

$$\begin{aligned}\|\hat{\boldsymbol{x}}_i^o(\tau|t_{p+1})\|_{\mathcal{P}_i} &\leqslant \|\hat{\boldsymbol{x}}_i^*(\tau|t_p)\|_{\mathcal{P}_i} + \eta_i(t_{p+1})e^{L_i(\tau-t_{p+1})} \\ &\leqslant \frac{\alpha_i H_p}{\tau-t_p}\boldsymbol{\varepsilon}_i + \eta_{\mathrm{ip}}^{\max}e^{L_i(t_p+H_p-t_{p+1})} \\ &\leqslant \frac{\alpha_i H_p}{\tau-t_p}\boldsymbol{\varepsilon}_i + (1-\alpha_i)\boldsymbol{\varepsilon}_i. \end{aligned} \tag{19}$$

On the time interval $\tau \in [t_{p+1}, t_p+H_p]$, in order to derive (i), it is equivalent to showing that

$$(1-\alpha_i)\boldsymbol{\varepsilon}_i \leqslant \frac{\alpha_i H_{p+1}}{\tau-t_{p+1}}\boldsymbol{\varepsilon}_i - \frac{\alpha_i H_p}{\tau-t_p}\boldsymbol{\varepsilon}_i. \tag{20}$$

Noting the definition of (6), the right part of (20) turns to

$$\begin{aligned}\frac{\alpha_i H_{p+1}}{\tau-t_{p+1}}\boldsymbol{\varepsilon}_i - \frac{\alpha_i H_p}{\tau-t_p}\boldsymbol{\varepsilon}_i &= \frac{(t_{p+1}-t_p)H_p - \mu_p(\tau-t_p)\left(H_p-H_p^*\right)}{(\tau-t_{p+1})(\tau-t_p)}\alpha_i\boldsymbol{\varepsilon}_i \\ &\geqslant \frac{\beta H_p - \mu_p\left(H_p-H_p^*\right)}{(1-\beta)H_p}\alpha_i\boldsymbol{\varepsilon}_i, \end{aligned} \tag{21}$$

where $(t_{p+1}-t_p)H_p - \mu_p(\tau-t_p)\left(H_p-H_p^*\right) \geqslant 0$ can be guaranteed in light of (14). As a consequence of condition (17) and inequalities (20) and (21), one can obtain $\|\hat{\boldsymbol{x}}_i^o(\tau|t_{p+1})\|_{\mathcal{P}_i} \leqslant \frac{\alpha_i H_{p+1}}{\tau-t_{p+1}}\boldsymbol{\varepsilon}_i$ for $\tau \in [t_{p+1}, t_p+H_p]$. Furthermore, it follows from (13) that $\hat{\boldsymbol{u}}_i^o(\tau|t_{p+1}) = \hat{\boldsymbol{u}}_i^*(\tau|t_p) \in \mathscr{U}_i$, $\tau \in [t_{p+1}, t_p+H_p]$.

Next, when $\tau \in [t_p + H_p, t_{p+1} + H_{p+1}]$, consider the feasible state trajectory $\hat{\boldsymbol{x}}_i^o(\tau|t_{p+1})$. By virtue of (16), we derive

$$\|\hat{\boldsymbol{x}}_i^o(\tau|t_{p+1})\|_{\mathcal{P}_i} \leqslant \boldsymbol{\varepsilon}_i e^{-\frac{\underline{\lambda}(\mathcal{Q}_i^*)}{2\bar{\lambda}(\mathcal{P}_i)}(\tau - t_p - H_p)}.$$

In order to prove $\|\hat{\boldsymbol{x}}_i^o(\tau|t_{p+1})\|_{\mathcal{P}_i} \leqslant \frac{\alpha_i H_{p+1}}{\tau - t_{p+1}}\boldsymbol{\varepsilon}_i$ for all $\tau \in [t_p + H_p, t_{p+1} + H_{p+1}]$, two functions $\mathcal{F}(\tau)$ and $g(\tau)$ are, respectively, defined as

$$\mathcal{F}(\tau) \triangleq \frac{\alpha_i H_{p+1}}{\tau - t_{p+1}}\boldsymbol{\varepsilon}_i - \boldsymbol{\varepsilon}_i e^{-\frac{\underline{\lambda}(\mathcal{Q}_i^*)}{2\bar{\lambda}(\mathcal{P}_i)}(\tau - t_p - H_p)} \tag{22}$$

and

$$g(\tau) \triangleq \alpha_i H_{p+1} e^{\frac{\underline{\lambda}(\mathcal{Q}_i^*)}{2\bar{\lambda}(\mathcal{P}_i)}(\tau - t_p - H_p)} - (\tau - t_{p+1}). \tag{23}$$

One can find from (22) and (23) that $\mathcal{F}(\tau) \geqslant 0$ holds if $g(\tau) \geqslant 0$ for $\tau \in [t_p + H_p, t_{p+1} + H_{p+1}]$. Hence, taking the derivative of $g(\tau)$, it turns to

$$\begin{aligned} g'(\tau) &= \frac{\alpha_i H_{p+1}\underline{\lambda}(\mathcal{Q}_i^*)}{2\bar{\lambda}(\mathcal{P}_i)} e^{\frac{\underline{\lambda}(\mathcal{Q}_i^*)}{2\bar{\lambda}(\mathcal{P}_i)}(\tau - t_p - H_p)} - 1 \\ &\leqslant \frac{\alpha_i H_{p+1}\underline{\lambda}(\mathcal{Q}_i^*)}{2\bar{\lambda}(\mathcal{P}_i)} e^{\frac{\underline{\lambda}(\mathcal{Q}_i^*)}{2\bar{\lambda}(\mathcal{P}_i)}H_{p+1}} - 1. \end{aligned}$$

Based on the condition in (18), it guarantees that $g(\tau)$ is a decreasing function for $[t_p + H_p, t_{p+1} + H_{p+1}]$. In addition, $g(t_{p+1} + H_{p+1}) \geqslant 0$ is straightforwardly satisfied under the condition in (14). Finally, the satisfaction of the constraint for the feasible input remains to demonstrate. Since $\hat{\boldsymbol{x}}_i^o(t_p + H_p|t_{p+1}) \in \Psi_i(\boldsymbol{\varepsilon}_i)$ holds by Lemma 3, Lemma 1 is available. It follows that $\hat{\boldsymbol{u}}_i^o(\tau|t_{p+1}) = \mathcal{K}_i\hat{\boldsymbol{x}}_i^o(\tau|t_{p+1}) \in \mathscr{U}_i$, $\tau \in [t_p + H_p, t_{p+1} + H_{p+1}]$.

Remark 9. In Theorem 2, the conditions established in (14), (17) and (18) determine the permissible range of the shrinkage factor μ_p, ensuring that the prediction horizon is appropriately shortened while maintaining the recursive feasibility of Algorithm 2.

4.2 Stability analysis

In this subsection, under the proposed DETMPC algorithm, the closed-loop stability of MASs is analyzed. To this end, Lemma 4 first proves that the state trajectory of each agent enters the terminal region in finite time. On this basis, Theorem 3 is subsequently employed to establish the closed-loop stability of each agent.

Lemma 4. Suppose Assumptions 1 and 2, and the conditions in Theorem 2 hold. For the i-th agent under the DETMPC algorithm, if $\boldsymbol{x}_i(t) \notin \Psi_i(\boldsymbol{\varepsilon}_i)$ and the following inequality is satisfied:

$$\begin{aligned} &\frac{\bar{\lambda}(\mathcal{Q}_i)}{\underline{\lambda}(\mathcal{P}_i)}\eta_{ip}^{\max}\left[\frac{\eta_{ip}^{\max} + \alpha_i\boldsymbol{\varepsilon}_i H_p}{2L_i}\left(e^{2L_i(1-\beta)H_p} - 1\right) + \frac{\alpha_i(1-\beta)\boldsymbol{\varepsilon}_i}{\beta}\right] \\ &\quad + (1-\alpha_i^2)\boldsymbol{\varepsilon}_i^2 + \sum_{j\in\mathcal{N}_i^{in}}\Pi_{ij} < \frac{\underline{\lambda}(\mathcal{Q}_i)}{\bar{\lambda}(\mathcal{P}_i)}(\boldsymbol{\varepsilon}_i - \eta_{ip}^{\max})^2\beta H_p, \end{aligned} \tag{24}$$

where $\Pi_{ij} = (\frac{\bar{\lambda}(\sqrt{\mathcal{Q}_{ij}})}{\underline{\lambda}(\sqrt{\mathcal{P}_i})}(\frac{\alpha_i\boldsymbol{\varepsilon}_i}{\beta} + (1-\alpha_i)\boldsymbol{\varepsilon}_i) + \frac{\bar{\lambda}(\sqrt{\mathcal{Q}_{ij}})\alpha_j\boldsymbol{\varepsilon}_j}{\underline{\lambda}(\sqrt{\mathcal{P}_j})\beta})^2(1-\beta)H_p + (\frac{\bar{\lambda}(\sqrt{\mathcal{Q}_{ij}})}{\underline{\lambda}(\sqrt{\mathcal{P}_i})}\boldsymbol{\varepsilon}_i + \frac{\bar{\lambda}(\sqrt{\mathcal{Q}_{ij}})}{\underline{\lambda}(\sqrt{\mathcal{P}_j})}\alpha_j\boldsymbol{\varepsilon}_j)^2 H_{p+1}$, then agent i will enter $\Psi_i(\boldsymbol{\varepsilon}_i)$ in finite time.

Proof. Let $\Delta\boldsymbol{J} \triangleq \boldsymbol{J}_i(\hat{\boldsymbol{x}}_i^o(\tau|t_{p+1}), \tilde{X}_i(\tau|t_{p+1}), \hat{\boldsymbol{u}}_i^o(\tau|t_{p+1})) - \boldsymbol{J}_i(\hat{\boldsymbol{x}}_i^*(\tau|t_p), \tilde{X}_i(\tau|t_p), \hat{\boldsymbol{u}}_i^*(\tau|t_p))$. Splitting the terms in $\Delta\boldsymbol{J}$, we have $\Delta\boldsymbol{J} = \sum_{l=1}^4 \Delta_l$, where

$$\begin{aligned} \Delta_1 &\triangleq \int_{t_p+H_p}^{t_{p+1}+H_{p+1}} \left(\|\hat{\boldsymbol{x}}_i^o(\xi|t_{p+1})\|_{\mathcal{Q}_i}^2 + \|\hat{\boldsymbol{u}}_i^o(\xi|t_{p+1})\|_{\mathcal{R}_i}^2\right)\mathrm{d}\xi \\ &\quad + \|\hat{\boldsymbol{x}}_i^o(t_{p+1} + H_{p+1}|t_{p+1})\|_{\mathcal{P}_i}^2 - \|\hat{\boldsymbol{x}}_i^*(t_p + H_p|t_p)\|_{\mathcal{P}_i}^2, \\ \Delta_2 &\triangleq \int_{t_{p+1}}^{t_p+H_p} \left(\|\hat{\boldsymbol{x}}_i^o(\xi|t_{p+1})\|_{\mathcal{Q}_i}^2 - \|\hat{\boldsymbol{x}}_i^*(\xi|t_p)\|_{\mathcal{Q}_i}^2\right)\mathrm{d}\xi, \\ \Delta_3 &\triangleq -\int_{t_p}^{t_{p+1}} \left(\|\hat{\boldsymbol{x}}_i^*(\xi|t_p)\|_{\mathcal{Q}_i}^2 + \|\hat{\boldsymbol{u}}_i^*(\xi|t_p)\|_{\mathcal{R}_i}^2\right)\mathrm{d}\xi, \end{aligned}$$

$$\Delta_4 \triangleq \int_{t_{p+1}}^{t_{p+1}+H_{p+1}} \sum_{j\in\mathcal{N}_i^{in}} \|\hat{\boldsymbol{x}}_i^o(\xi|t_{p+1}) - \tilde{\boldsymbol{x}}_j(\xi|t_{p+1})\|_{\mathcal{Q}_{ij}}^2 \,\mathrm{d}\xi - \int_{t_p}^{t_p+H_p} \sum_{j\in\mathcal{N}_i^{in}} \|\hat{\boldsymbol{x}}_i^*(\xi|t_p) - \tilde{\boldsymbol{x}}_j(\xi|t_p)\|_{\mathcal{Q}_{ij}}^2 \,\mathrm{d}\xi.$$

According to Lemma 1, we obtain that $\|\hat{\boldsymbol{x}}_i^o(\tau|t_{p+1})\|_{Q_i^*}^2 \leqslant -\dot{V}_i(\hat{\boldsymbol{x}}_i^o(\tau|t_{p+1}))$ holds for $\tau \in [t_p+H_p, t_{p+1}+H_{p+1}]$. Then, one has

$$\begin{aligned}\Delta_1 \leqslant& \|\hat{\boldsymbol{x}}_i^o(t_p+H_p|t_{p+1})\|_{\mathcal{P}_i}^2 - \|\hat{\boldsymbol{x}}_i^*(t_p+H_p|t_p)\|_{\mathcal{P}_i}^2 \\ \leqslant& (1-\alpha_i^2)\boldsymbol{\varepsilon}_i^2.\end{aligned} \tag{25}$$

Considering Δ_2, it yields

$$\Delta_2 \leqslant \frac{\bar{\lambda}(\mathcal{Q}_i)}{\underline{\lambda}(\mathcal{P}_i)} \int_{t_{p+1}}^{t_p+H_p} \|\hat{\boldsymbol{x}}_i^o(\xi|t_{p+1}) - \hat{\boldsymbol{x}}_i^*(\xi|t_p)\|_{\mathcal{P}_i} (\|\hat{\boldsymbol{x}}_i^o(\xi|t_{p+1})\|_{\mathcal{P}_i} + \|\hat{\boldsymbol{x}}_i^*(\xi|t_p)\|_{\mathcal{P}_i}) \mathrm{d}\xi.$$

With the robustness constraint (5) and the inequalities (15) and (19) in mind, Δ_2 turns to

$$\begin{aligned}\Delta_2 \leqslant& \frac{\bar{\lambda}(\mathcal{Q}_i)}{\underline{\lambda}(\mathcal{P}_i)} \int_{t_{p+1}}^{t_p+H_p} \eta_{ip}^{\max} e^{L_i(\xi-t_{p+1})} \left[\frac{2\alpha_i H_p}{\xi-t_p}\boldsymbol{\varepsilon}_i + \eta_{ip}^{\max} e^{L_i(\xi-t_{p+1})}\right] \mathrm{d}\xi \\ \leqslant& \frac{\bar{\lambda}(\mathcal{Q}_i)}{\underline{\lambda}(\mathcal{P}_i)} \eta_{ip}^{\max} \left[\frac{\eta_{ip}^{\max} + \alpha_i\boldsymbol{\varepsilon}_i H_p}{2L_i}\left(e^{2L_i(1-\beta)H_p} - 1\right) + \frac{\alpha_i(1-\beta)\boldsymbol{\varepsilon}_i}{\beta}\right].\end{aligned} \tag{26}$$

For Δ_3, since $\boldsymbol{x}_i(t) \notin \Psi_i(\boldsymbol{\varepsilon}_i)$, utilizing the triggering scheme in (9) and the triangle inequality, we can deduce that

$$\begin{aligned}\Delta_3 \leqslant& -\frac{\underline{\lambda}(\mathcal{Q}_i)}{\bar{\lambda}(\mathcal{P}_i)} \int_{t_p}^{t_{p+1}} \|\hat{\boldsymbol{x}}_i^*(\xi|t_p)\|_{\mathcal{P}_i}^2 \,\mathrm{d}\xi \\ \leqslant& -\frac{\underline{\lambda}(\mathcal{Q}_i)}{\bar{\lambda}(\mathcal{P}_i)} (\boldsymbol{\varepsilon}_i - \eta_{ip}^{\max})^2 \beta H_p.\end{aligned} \tag{27}$$

For Δ_4, by virtue of the triangle inequality, one has

$$\begin{aligned}\Delta_4 \leqslant& \int_{t_{p+1}}^{t_{p+1}+H_{p+1}} \sum_{j\in\mathcal{N}_i^{in}} \|\hat{\boldsymbol{x}}_i^o(\xi|t_{p+1}) - \tilde{\boldsymbol{x}}_j(\xi|t_{p+1})\|_{\mathcal{Q}_{ij}}^2 \,\mathrm{d}\xi \\ \leqslant& \sum_{j\in\mathcal{N}_i^{in}} \left[\int_{t_{p+1}}^{t_p+H_p} \left(\|\hat{\boldsymbol{x}}_i^o(\xi|t_{p+1})\|_{\mathcal{Q}_{ij}} + \|\tilde{\boldsymbol{x}}_j(\xi|t_{p+1})\|_{\mathcal{Q}_{ij}}\right)^2 \mathrm{d}\xi \right. \\ &\left. + \int_{t_p+H_p}^{t_{p+1}+H_{p+1}} \left(\|\hat{\boldsymbol{x}}_i^o(\xi|t_{p+1})\|_{\mathcal{Q}_{ij}} + \|\tilde{\boldsymbol{x}}_j(\xi|t_{p+1})\|_{\mathcal{Q}_{ij}}\right)^2 \mathrm{d}\xi\right].\end{aligned}$$

Analogous to (19), on the time interval $\tau \in [t_{p+1}, t_p+H_p]$, there exists

$$\|\hat{\boldsymbol{x}}_i^o(\tau|t_{p+1})\|_{\mathcal{Q}_{ij}} \leqslant \frac{\bar{\lambda}(\sqrt{\mathcal{Q}_{ij}})}{\underline{\lambda}(\sqrt{\mathcal{P}_i})} \left(\frac{\alpha_i\boldsymbol{\varepsilon}_i}{\beta} + (1-\alpha_i)\boldsymbol{\varepsilon}_i\right).$$

Based on the definition (4), one yields

$$\|\tilde{\boldsymbol{x}}_j(\tau|t_{p+1})\|_{\mathcal{Q}_{ij}} \leqslant \frac{\bar{\lambda}(\sqrt{\mathcal{Q}_{ij}})\alpha_j\boldsymbol{\varepsilon}_j}{\underline{\lambda}(\sqrt{\mathcal{P}_j})\beta}, \tau \in [t_{p+1}, t_p+H_p].$$

Due to the facts that $\hat{\boldsymbol{x}}_i^o(\tau|t_{p+1}) \in \Psi_i(\boldsymbol{\varepsilon}_i)$ and $\tilde{\boldsymbol{x}}_j(\tau|t_{p+1}) \in \Psi_j(\alpha_j\boldsymbol{\varepsilon}_j)$ for $\tau \in [t_p+H_p, t_{p+1}+H_{p+1}]$, we, respectively, derive that

$$\|\hat{\boldsymbol{x}}_i^o(\tau|t_{p+1})\|_{\mathcal{Q}_{ij}} \leqslant \frac{\bar{\lambda}(\sqrt{\mathcal{Q}_{ij}})}{\underline{\lambda}(\sqrt{\mathcal{P}_i})}\boldsymbol{\varepsilon}_i$$

and

$$\|\tilde{\boldsymbol{x}}_j(\tau|t_{p+1})\|_{\mathcal{Q}_{ij}} \leqslant \frac{\bar{\lambda}(\sqrt{\mathcal{Q}_{ij}})}{\underline{\lambda}(\sqrt{\mathcal{P}_j})}\alpha_j\boldsymbol{\varepsilon}_j.$$

Based on the above analysis, Δ_4 turns to

$$\begin{aligned}\Delta_4 \leqslant \sum_{j\in\mathcal{N}_i^{in}}\Bigg[&\left(\frac{\bar{\lambda}(\sqrt{\mathcal{Q}_{ij}})}{\underline{\lambda}(\sqrt{\mathcal{P}_i})}\left(\frac{\alpha_i\boldsymbol{\varepsilon}_i}{\beta}+(1-\alpha_i)\boldsymbol{\varepsilon}_i\right)+\frac{\bar{\lambda}(\sqrt{\mathcal{Q}_{ij}})\alpha_j\boldsymbol{\varepsilon}_j}{\underline{\lambda}(\sqrt{\mathcal{P}_j})\beta}\right)^2\\&\cdot(1-\beta)H_p+\left(\frac{\bar{\lambda}(\sqrt{\mathcal{Q}_{ij}})}{\underline{\lambda}(\sqrt{\mathcal{P}_i})}\boldsymbol{\varepsilon}_i+\frac{\bar{\lambda}(\sqrt{\mathcal{Q}_{ij}})}{\underline{\lambda}(\sqrt{\mathcal{P}_j})}\alpha_j\boldsymbol{\varepsilon}_j\right)^2H_{p+1}\Bigg].\end{aligned}\tag{28}$$

Submitting (25)–(28) into $\Delta\boldsymbol{J}$, it arrives at

$$\begin{aligned}\Delta\boldsymbol{J}\leqslant&(1-\alpha_i^2)\boldsymbol{\varepsilon}_i^2-\frac{\underline{\lambda}(\mathcal{Q}_i)}{\bar{\lambda}(\mathcal{P}_i)}(\boldsymbol{\varepsilon}_i-\eta_{ip}^{\max})^2\beta H_p+\sum_{j\in\mathcal{N}_i^{in}}\Pi_{ij}\\&+\frac{\bar{\lambda}(\mathcal{Q}_i)}{\underline{\lambda}(\mathcal{P}_i)}\eta_{ip}^{\max}\left[\frac{\eta_{ip}^{\max}+\alpha_i\boldsymbol{\varepsilon}_iH_p}{2L_i}\left(e^{2L_i(1-\beta)H_p}-1\right)+\frac{\alpha_i(1-\beta)\boldsymbol{\varepsilon}_i}{\beta}\right].\end{aligned}\tag{29}$$

Finally, one gets $\boldsymbol{J}_i(\hat{\boldsymbol{x}}_i^*(\tau|t_{p+1}),\tilde{X}_i(\tau|t_{p+1}),\hat{\boldsymbol{u}}_i^*(\tau|t_{p+1}))-\boldsymbol{J}_i(\hat{\boldsymbol{x}}_i^*(\tau|t_p),\tilde{X}_i(\tau|t_p),\hat{\boldsymbol{u}}_i^*(\tau|t_p))\leqslant\Delta\boldsymbol{J}<0$ from condition (24), which means the cost function is strictly decreasing over time. Consequently, with the aid of technique in [36], the state of the i-th agent can enter $\Psi_i(\boldsymbol{\varepsilon}_i)$ in finite time.

Theorem 3. Suppose Assumptions 1 and 2, conditions in Theorem 2, and Eq. (24) hold. If the disturbance satisfies $\varrho_i\leqslant\frac{\underline{\lambda}(\mathcal{Q}_i^*)\boldsymbol{\varepsilon}_i}{2\bar{\lambda}(\mathcal{P}_i)\bar{\lambda}(\sqrt{\mathcal{P}_i})}$ for the i-th agent under the DETMPC algorithm, then the i-th agent state converges to the terminal region $\Psi_i(\boldsymbol{\varepsilon}_i)$.

Proof. For agent i in MASs, the discussion is split into the following two cases.

Case 1: $\boldsymbol{x}_i(t_0)\in\Psi_i(\boldsymbol{\varepsilon}_i)$. In this case, we suppose that $\boldsymbol{x}_i(t_0)\in\Psi_i(\boldsymbol{\varepsilon}_i)$ and $\boldsymbol{x}_i(t)\notin\Psi_i(\boldsymbol{\varepsilon}_i)$. That is, there exist $t>t_0$ and $\bar{\rho}>0$ such that the inequality $V_i(\boldsymbol{x}_i(t))\geqslant\boldsymbol{\varepsilon}_i^2+\bar{\rho}$ holds. Without loss of generality, let $t_\xi=\inf\{t\geqslant t_0: V_i(\boldsymbol{x}_i(t))\geqslant\boldsymbol{\varepsilon}_i^2+\bar{\rho}\}$, which is the minimum time for $\boldsymbol{x}_i(t)\notin\Psi_i(\boldsymbol{\varepsilon}_i)$. Then, taking the Lyapunov function candidate as $V_i(\boldsymbol{x}_i(t))=\boldsymbol{x}_i^\top(t)\mathcal{P}_i\boldsymbol{x}_i(t)$, the derivative of $V_i(\boldsymbol{x}_i(t))$ along the dynamics of (1) follows

$$\begin{aligned}\dot{V}_i(\boldsymbol{x}_i(t))\leqslant&-\|\boldsymbol{x}_i(t)\|_{\mathcal{Q}_i^*}^2+2\boldsymbol{x}_i^\top(t)\mathcal{P}_i\boldsymbol{\omega}_i(t)\\\leqslant&-\|\boldsymbol{x}_i(t)\|_{\mathcal{Q}_i^*}^2+2\|\boldsymbol{x}_i(t)\|_{\mathcal{P}_i}\|\boldsymbol{\omega}_i(t)\|_{\mathcal{P}_i}.\end{aligned}$$

According to $\varrho_i\leqslant\frac{\underline{\lambda}(\mathcal{Q}_i^*)\boldsymbol{\varepsilon}_i}{2\bar{\lambda}(\mathcal{P}_i)\bar{\lambda}(\sqrt{\mathcal{P}_i})}$, one has $\dot{V}_i(\boldsymbol{x}_i(t))\leqslant0$. Thus, there exists a time instant $t'_\xi\in(t_0,t_\xi)$ such that $\boldsymbol{\varepsilon}_i^2+\bar{\rho}\leqslant V_i(\boldsymbol{x}_i(t_\xi))\leqslant V_i(\boldsymbol{x}_i(t'_\xi))$, which contradicts the definition of t_ξ. This indicates that the dual-mode control strategy ensures the state of the closed-loop system remains stable within the terminal set under the terminal state-feedback controller.

Case 2: $\boldsymbol{x}_i(t_0)\notin\Psi_i(\boldsymbol{\varepsilon}_i)$. Applying Lemma 4, agent i will be inside the region $\Psi_i(\boldsymbol{\varepsilon}_i)$ in finite time. We then follow the same arguments in Case 1 that the i-th agent can be stabilized within the region $\Psi_i(\boldsymbol{\varepsilon}_i)$.

Remark 10. With the aid of the robustness constraint (5), condition (24) is established to ensure that the optimal cost function always decreases over time. Based on this, the sufficient conditions for the closed-loop stability of MASs are formulated in Theorem 3. It is noteworthy that in (24), the stability is primarily associated with the shrinkage coefficient μ_p, the upper bound of the triggering threshold $\eta_{ip}^{\max}$, the terminal region $\boldsymbol{\varepsilon}_i$, the cooperation term Π_{ij}, and the disturbance bound ϱ_i. For the given system parameters, condition (24) establishes the permissible range of μ_p that guarantees closed-loop stability and effectively reduces the prediction horizon.

5 Numerical example

In this simulation, we utilize the MASs consisting of three nonlinear agents in [30, 31] to validate the proposed algorithm, where the i-th agent is given by

$$\begin{cases}\dot{\boldsymbol{x}}_{i1}(t)=\boldsymbol{x}_{i2}(t)+\boldsymbol{u}_i(t)(\delta_i-(1-\delta_i)\boldsymbol{x}_{i1}(t))+\boldsymbol{\omega}_{i1}(t),\\\dot{\boldsymbol{x}}_{i2}(t)=\boldsymbol{x}_{i1}(t)+\boldsymbol{u}_i(t)(\delta_i-4(1-\delta_i)\boldsymbol{x}_{i2}(t))+\boldsymbol{\omega}_{i2}(t),\end{cases}$$

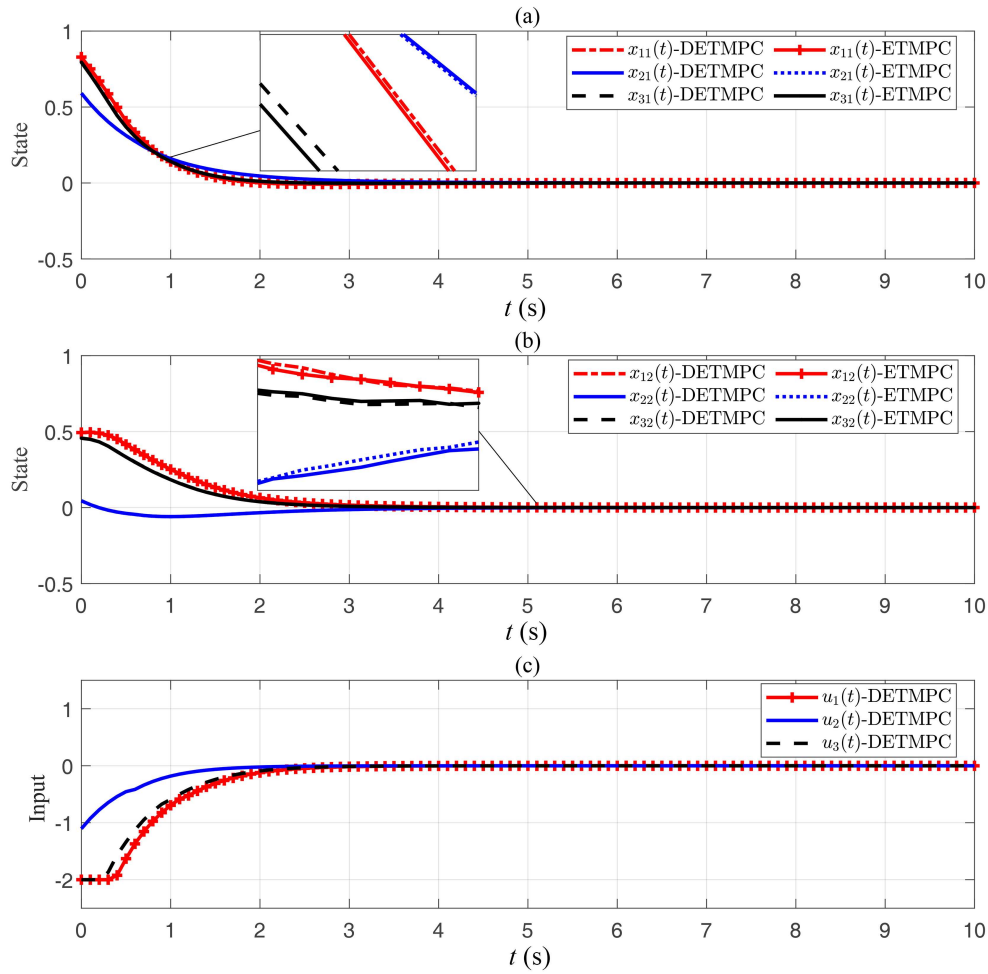

Figure 2 (Color online) (a) States $\boldsymbol{x}_{i1}(t)$ of three agents under the DETMPC and ETMPC schemes. (b) States $\boldsymbol{x}_{i2}(t)$ of three agents under the DETMPC and ETMPC schemes. (c) Control input $\boldsymbol{u}_i(t)$ of three agents under the DETMPC scheme.

where $i = 1, 2, 3$, $\boldsymbol{x}_i(t) = [\boldsymbol{x}_{i1}(t), \boldsymbol{x}_{i2}(t)]^\top \in \mathbb{R}^2$, $\boldsymbol{u}_i(t) \in \mathbb{R}^1$, $\boldsymbol{\omega}_i(t) = [\boldsymbol{\omega}_{i1}(t), \boldsymbol{\omega}_{i2}(t)]^\top \in \mathbb{R}^2$ and $\delta_i \in (0, 1)$ is the nonlinear degree for agent i. For simplicity, all agents share identical system parameters. Furthermore, agent 1, agent 2, and agent 3 have access to the information from agent 2, agent 3, and agent 1, respectively.

For the i-th nonlinear agent, let the control input be constrained by $|\boldsymbol{u}_i(t)| \leqslant 2$, and the nonlinear degree is set as $\delta_i = 0.8$. We select $\mathcal{Q}_i = [0.1, 0; 0, 0.1]$, $\mathcal{Q}_{ij} = [0.0001, 0; 0, 0.0001]$, and $\mathcal{R}_i = 0.05$. Using the LQR approach, the state feedback gain and the terminal matrix are determined as $\mathcal{K}_i = [-1.8042, -1.8042]$ and $\mathcal{P}_i = [0.0814, 0.0314; 0.03140.0814]$, respectively. The Lipschitz constant $L_i = 0.13$ can be correspondingly calculated by [35]. Set $t_0 = 0$, $\beta = 0.23$, $\boldsymbol{\varepsilon}_i = 0.08$, $\alpha_i = 0.995$, and H_0=1.3 s. The sampling time is 0.1 s. The initial value of each agent is presented as $\boldsymbol{x}_{10} = [0.8287, 0.4938]^\top$, $\boldsymbol{x}_{20} = [0.5907, 0.0449]^\top$, and $\boldsymbol{x}_{30} = [0.7948, 0.4568]^\top$. The related parameters of the dynamic event-triggered mechanism (9) for agent i are given as $a_i = 0.3$, $b_i = 0.7$, $\eta_{i0}^{\max} = 3.5119 \times 10^{-4}$ and $\eta_i(t_0) = \eta_{i0}^{\min} = 1.0040 \times 10^{-5}$. The upper bound of the external disturbance is derived as $\varrho_i \leqslant 0.0034$ from Lemma 2 and Theorem 3. Here, we set that $\varrho_i = 0.001$. Based on the sufficient conditions established in our work, we set $\mu_p = 0.4 + 0.05\sin(t_p)$ to ensure the recursive feasibility and closed-loop stability.

For comparison purposes, we conduct the ETMPC scheme in [16] under the static triggering threshold $\eta_i(t_0)$, and the same system parameters. Particularly, the above numerical experiments are implemented by using the fmincon function in Matlab R2023a with 4.00 GHz AMD Ryzen 9 8945HS CPU. The corresponding numerical results are shown in Figures 2–4 and Table 1. In Figures 2(a) and (b), the formation stabilization is achieved under the proposed DETMPC scheme, resulting in performance comparable to that of the scheme in [16]. In addition, the control input trajectories under the DETMPC algorithm of each agent are given in Figure 2(c), where the constraints for system input are satisfied. In Figure 3, the triggering instants, the corresponding prediction horizons and the trajectories of triggering threshold for each agent are shown, where $\eta_{\min}(t) = \max_{i\in\mathcal{V}}\{\eta_i^{\min}(t)\}$ and $\eta_{\max}(t) = \min_{i\in\mathcal{V}}\{\eta_i^{\max}(t)\}$. Under the dynamic event-triggered mechanism in (9), the proposed DETMPC reduces the triggering frequency and

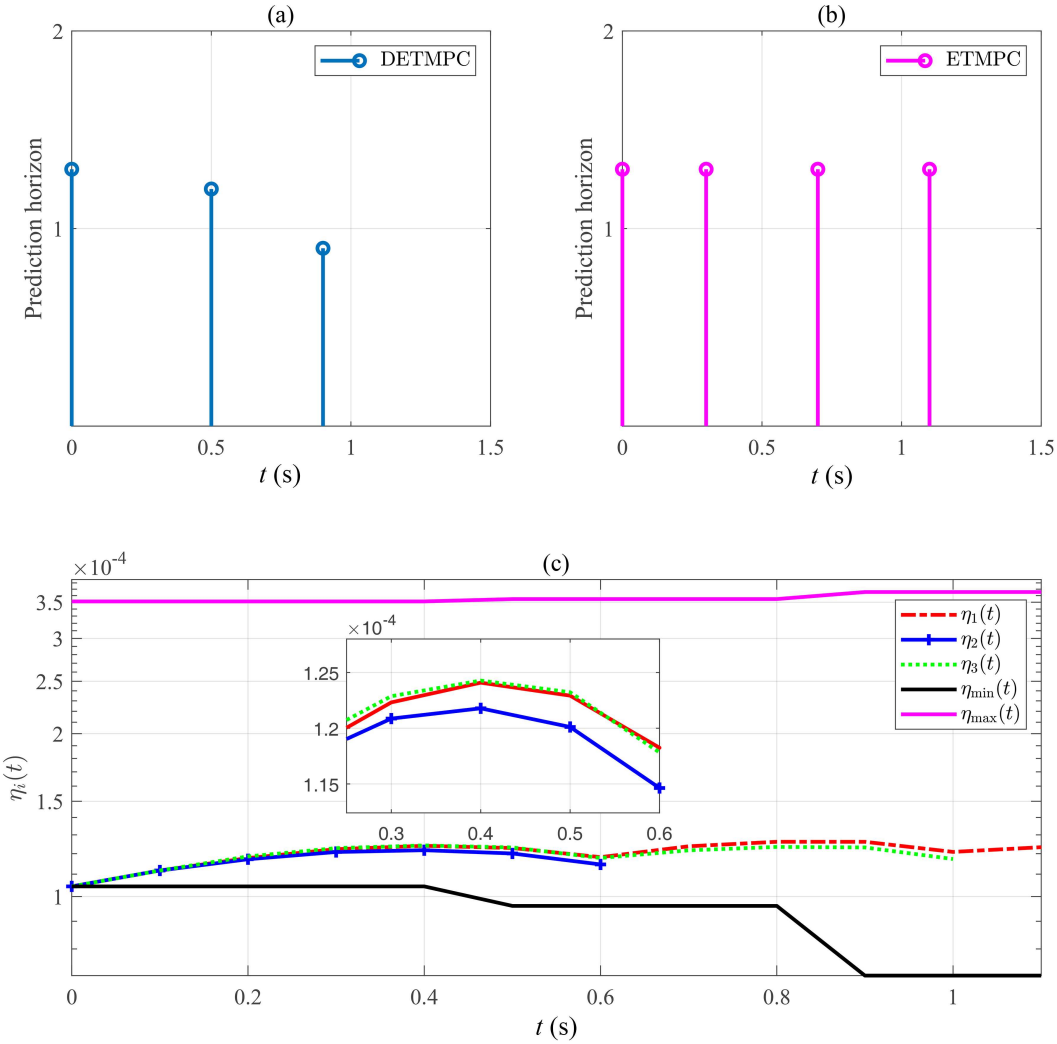

Figure 3 (Color online) (a) Triggering instants and prediction horizons under the DETMPC algorithm; (b) triggering instants and prediction horizons under the algorithm in [16]; (c) trajectories of the triggering threshold for the MASs with the event-triggered scheme in (9).

Table 1 Performance comparison.

Strategy	μ_p	Triggering numbers	Solving time (s)	Cost
DETMPC	0.45	3	0.529	0.5214
DETMPC	0.2	3	0.614	0.5627
DETMPC	0.1	3	0.657	0.5730
ETMPC in [16]	$*$	4	0.852	0.6473

achieves a larger inter-event interval compared with the scheme in [16]. This aligns with the results in Proposition 1 and reduces the computational resources. Meanwhile, the inter-event time interval is strictly larger than βH_p, as shown in Figure 3(a). Furthermore, unlike the static prediction horizon in [16], the proposed algorithm adaptively shortens the prediction horizon according to the shrinkage mechanism in (6), effectively reducing the computational resources.

Then, with respect to the shrinkage parameter μ_p, triggering numbers, total solving time and the total cost calculated by the cost function in the optimization problem, the comparison results are summarized in Table 1. As shown in Table 1 and Figure 2(a), the proposed algorithm can effectively reduce the computational resources while guaranteeing satisfactory control performance compared with the existing ETMPC algorithm [16]. Meanwhile, considering the proposed algorithm under the different shrinkage coefficient μ_p, the system performance with regard to the runtime of the optimization is presented in Table 1, which means the performance can be flexibly adjusted by the proposed algorithm.

In case the terminal region is too small, the DETMPC approach proposed herein can be applied throughout

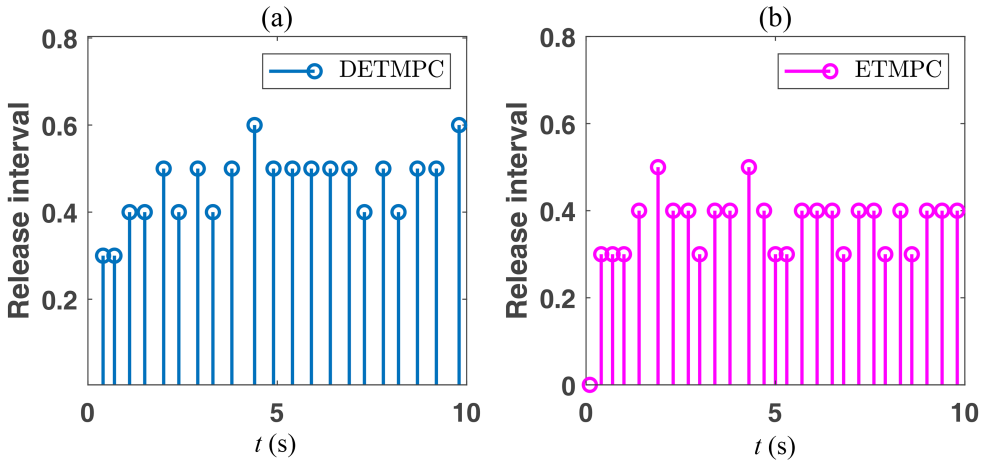

Figure 4 (Color online) (a) Triggering instants and release intervals under the proposed DETMPC scheme (22 triggers); (b) triggering instants and release intervals under the algorithm in [16] (27 triggers).

the entire control process. This aligns with the consideration in [34], which highlights the need for an efficient event-triggered scheme for the MPC problem. As a result, a further comparative analysis focusing on the event-triggered scheme is carried out and the results are presented in Figure 4. It can be seen that the proposed DETMPC algorithm has 22 triggers, whereas the scheme in [16] results in 27 triggers. As a consequence, the proposed scheme can reduce the computational resources. In addition, from Figure 4, a larger inter-execution interval is achieved under the developed scheme, which is in accordance with the analysis in Proposition 1.

6 Conclusion

This article presents a DETMPC algorithm for nonlinear MASs subject to control input constraints and external disturbances. The proposed dynamic event-triggered mechanism effectively reduces the frequency of solving the optimization problems, thereby decreasing the computational burden of the algorithm. Additionally, a prediction-horizon shrinkage mechanism is incorporated to further improve computational efficiency. To enhance robustness against disturbances, a robustness constraint combined with the shrinkage strategy is embedded into the optimization problem. Furthermore, sufficient conditions have been rigorously derived to guarantee both the recursive feasibility and closed-loop stability of the overall system. The effectiveness of the proposed approach has been validated through a numerical example and comparative studies. Since data-driven techniques can further enhance the practical applications of the proposed algorithm by reducing the reliance on accurate models, the development of a data-driven DETMPC scheme for nonlinear MASs constitutes a promising and challenging direction for future research.

Acknowledgements This work was supported by National Natural Science Foundation of China (Grant Nos. 62473265, 62476176, 62576223, 12426311).

References

1 Xiong X L, Yang X S, Cao J D, et al. Finite-time control for a class of hybrid systems via quantized intermittent control. Sci China Inf Sci, 2020, 63: 192201
2 Mao B, Wu X, Fan Z, et al. Performance-guaranteed finite-time tracking of strict-feedback systems with unknown control directions: a novel switching mechanism. IEEE Trans Automat Contr, 2025, 70: 4061–4068
3 Jin X, Ho D W C, Tang Y. Synchronization of multiple rigid body systems: a survey. Chaos, 2023, 33: 092102
4 Zou A M, Kumar K D. Neural network-based distributed attitude coordination control for spacecraft formation flying with input saturation. IEEE Trans Neural Netw Learn Syst, 2012, 23: 1155–1162
5 Wu X Q, Wu X Q, Wang C Y, et al. Synchronization in multiplex networks. Phys Rep, 2024, 1060: 1–54
6 Xu Y, Wang J, Xia C Y, et al. Higher-order temporal interactions promote the cooperation in the multiplayer snowdrift game. Sci China Inf Sci, 2023, 66: 222208
7 Bharadwaj S, Carr S, Neogi N, et al. Decentralized control synthesis for air traffic management in urban air mobility. IEEE Trans Control Netw Syst, 2021, 8: 598–608
8 Yu W W, Chen D X, Liu H Z, et al. Systems science in the new era: intelligent systems and big data. Sci China Inf Sci, 2024, 67: 136201
9 Lu Q, Liao X, Li H, et al. Achieving acceleration for distributed economic dispatch in smart grids over directed networks. IEEE Trans Netw Sci Eng, 2020, 7: 1988–1999
10 Qian F, Du W L, Zhong W M, et al. Artificial intelligence-assisted design of new chemical materials: a perspective. Sci China Inf Sci, 2024, 67: 186201
11 Guo R, Feng J, Wang J, et al. Event-triggered adaptive horizon DMPC for discrete-time coupled nonlinear systems. IEEE CAA J Autom Sin, 2025, 12: 1724–1726
12 Li H, Zhan J, Zhang H T, et al. Distributed model predictive consensus of constrained heterogeneous multiagent systems. IEEE Trans Syst Man Cybern Syst, 2023, 53: 4155–4164

13 Yi C B, Cai J Y, Guo R. Synchronization of a class of nonlinear multiple neural networks with delays via a dynamic event-triggered impulsive control strategy. Electron Res Arch, 2024, 32: 4581–4603
14 Ruan X, Xu F, Xiang Y, et al. Dynamic event-triggered consensus control of multiagent systems under DoS attacks with intermittent communication. Asian J Control, 2025, doi: 10.1002/asjc.3875
15 Wang X, Sun J, Deng F, et al. Event-triggered consensus control of heterogeneous multi-agent systems: model- and data-based approaches. Sci China Inf Sci, 2023, 66: 192201
16 Li H, Shi Y. Event-triggered robust model predictive control of continuous-time nonlinear systems. Automatica, 2014, 50: 1507–1513
17 Zhou Y, Li D, Xi Y, et al. Event-triggered distributed robust model predictive control for a class of nonlinear interconnected systems. Automatica, 2022, 136: 110039
18 Sun Q, Chen J C, Shi Y. Event-triggered robust MPC of nonlinear cyber-physical systems against DoS attacks. Sci China Inf Sci, 2022, 65: 110202
19 Zou Y, Su X, Li S, et al. Event-triggered distributed predictive control for asynchronous coordination of multi-agent systems. Automatica, 2019, 99: 92–98
20 Shi T, Shi P, Wu Z G. Dynamic event-triggered asynchronous MPC of Markovian jump systems with disturbances. IEEE Trans Cybern, 2021, 52: 11639–11648
21 Sun Z, Li C, Zhang J, et al. Dynamic event-triggered MPC with shrinking prediction horizon and without terminal constraint. IEEE Trans Cybern, 2021, 52: 12140–12149
22 Li B, Zhou X, Ning Z, et al. Dynamic event-triggered security control for networked control systems with cyber-attacks: a model predictive control approach. Inf Sci, 2022, 612: 384–398
23 Li H, Yan W, Shi Y, et al. Periodic event-triggering in distributed receding horizon control of nonlinear systems. Syst Control Lett, 2015, 86: 16–23
24 Zhou Y, Li D, Xi Y, et al. Periodic event-triggered control for distributed networked multiagents with asynchronous communication: a predictive control approach. Intl J Robust Nonlinear, 2019, 29: 43–66
25 Liu Y, Chen Y, Li M. Dynamic event-based model predictive load frequency control for power systems under cyber attacks. IEEE Trans Smart Grid, 2021, 12: 715–725
26 Liu C, Li H, Shi Y, et al. Codesign of event trigger and feedback policy in robust model predictive control. IEEE Trans Automat Contr, 2020, 65: 302–309
27 Wang P B, Ren X M, Zheng D D. Robust nonlinear MPC with variable prediction horizon: an adaptive event-triggered approach. IEEE Trans Automat Contr, 2023, 68: 3806–3813
28 Sun Z, Dai L, Liu K, et al. Robust self-triggered MPC with adaptive prediction horizon for perturbed nonlinear systems. IEEE Trans Automat Contr, 2019, 64: 4780–4787
29 Hashimoto K, Adachi S, Dimarogonas D V. Event-triggered intermittent sampling for nonlinear model predictive control. Automatica, 2017, 81: 148–155
30 Zhan J, Hu Y, Li X. Adaptive event-triggered distributed model predictive control for multi-agent systems. Syst Control Lett, 2019, 134: 104531
31 Yang H, Zhao H, Xia Y, et al. Event-triggered active MPC for nonlinear multiagent systems with packet losses. IEEE Trans Cybern, 2021, 51: 3093–3102
32 Li H, Shi Y. Robust distributed model predictive control of constrained continuous-time nonlinear systems: a robustness constraint approach. IEEE Trans Automat Contr, 2013, 59: 1673–1678
33 Du S, Zhao M, Wang X, et al. Dual-mode event-triggered predictive control for nonlinear systems with bounded disturbances. Intl J Robust Nonlinear, 2024, 34: 1878–1897
34 Liu C, Li H, Shi Y, et al. Distributed event-triggered model predictive control of coupled nonlinear systems. SIAM J Control Optim, 2020, 58: 714–734
35 Khalil H K. Nonlinear Systems. 3rd ed. Upper Saddle River: Prentice-Hall, 2002
36 Michalska H, Mayne D Q. Robust receding horizon control of constrained nonlinear systems. IEEE Trans Automat Contr, 1993, 38: 1623–1633